IEEE Access
Multidisciplinary | Rapid Review | Open Access Journal

Received January 29, 2019, accepted February 21, 2019, date of publication March 11, 2019, date of current version March 25, 2019.

Digital Object Identifier 10.1109/ACCESS.2019.2903488

Algorithms and Instrument for Rapid Detection of Rail Surface Defects and Vertical Short-Wave Irregularities Based on FOG and Odometer

CUIJUN DONG[1], QINGZHOU MAO[2,3], XIAOCHUN REN[4], DONGHUA KOU[5], JIE QIN[5], AND WEI HU[1]

[1]State Key Laboratory of Information Engineering in Surveying, Mapping and Remote Sensing, Wuhan University, Wuhan 430079, China
[2]School of Remote Sensing and Information Engineering, Wuhan University, Wuhan 430079, China
[3]Engineering Research Center for Spatial-Temporal Data Smart Acquisition and Application, Ministry of Education of China, Wuhan University, Wuhan 430079, China
[4]State Key Laboratory of Rail Transit Engineering Information (FSDI), Xi'an 710043, China
[5]Wuhan Railway Administration Group, Co., Ltd., Wuhan 430071, China

Corresponding author: Qingzhou Mao (qzhmao@whu.edu.cn)

This work was supported in part by the Fundamental Research Funds for the Central Universities under Grant 2042017kf0235, and in part by the National Key Research Program under Grant 2016YFF0103502.

ABSTRACT Defects and vertical short-wave irregularities significantly influence the maintenance of the railway tracks and the train safety, and hence, they need to be detected and eliminated in the early stages of formation. We studied the principles and algorithms to detect the defects and to measure the vertical short-wave irregularities by using a fiber optical gyroscope and an odometer, and the associated software was also developed. The principles of deformation index, namely, the ratio of angular rate to velocity and the method to determine the threshold of defects detection, are expatiated. The influence of the transfer function in measuring the vertical irregularities has long been a tough issue. The relation between the characteristics of deformation index and the wavelength of irregularities is studied by converting the deformation index from the time domain to the spatial domain. The post-processing module utilizes the results of the spectrum analysis of the deformation index to determine the wavelength of the track irregularities and eliminate the influence of the transfer function. To improve the accuracy of the calculation results, we analyzed the characteristics of the output of the gyroscope and the odometer and designed a series of targeted error-elimination methods. The forward and reverse dead-reckoning method is utilized to reduce the error accumulation, especially a high frequency noise when calculating the magnitude of the vertical short-wave irregularities. The experimental results show that the repeatability is 0.038 mm when the chord length is 1 m and 0.65 mm when the chord length is 10 m. The accuracy is 0.05 mm when compared with the results obtained using a ruler of 1 m. The moving speed of the instrument was approximately 0.6–1.2 m/s during the experiment. Both the accuracy and the efficiency can fulfill the requirements for the measurement of the short-wave irregularities.

INDEX TERMS Fiber optical gyro, short-wave irregularity, deformation index, transfer function, dead reckoning.

I. INTRODUCTION

A. BACKGROUND

Vertical track irregularities refer to the deviations between the designed values and actual values of the rail surface's geometry of railway track. Among which, the wavelength of short-wave irregularities is less than 1 m and the amplitudes are less than 2 mm [1]. Figure 1 and Figure 2 [2] shows examples of defects and short-wave irregularities on the rail surface.

The presence of defects and short-wavelength track irregularities not only cause the unnecessary noises and vibrations that bring discomfort to train passengers, but also increase the interaction force between wheels and rails, which

The associate editor coordinating the review of this manuscript and approving it for publication was Lubin Chang.

FIGURE 1. Defects on rail surfaces.

FIGURE 2. Irregularities on rail surfaces.

results in reduction of the lifetime of railway tracks, associated instruments, instability of the train and possibility of derailment [3]–[6]. According to practical experience, track irregularities must be eliminated in the early stages of its formation, otherwise it can deteriorate rapidly. Thus, how to measure vertical irregularities efficiently and precisely is a key issue in the maintenance and repair of railway tracks [5]–[7].

B. CURRENT RESEARCH STATUS

The instruments developed for the detection of short-wave irregularities can be classified into two categories according to the techniques used, and include the mid-chord offset method and inertial reference method [7]–[8].

1) INSTRUMENTS BASED ON THE MID-CHORD OFFSET METHOD

This type of instrument generally requires setting up a measurement baseline and then measuring the deviation between the rail surface and the baseline. For instance, a Dutch company developed an instrument namely, RailProf, which utilizes the framework of this instrument to set up the baseline of measurement and measures the deviations directly by using a vertical distance sensor [9]. Shen *et al.* [10] developed an instrument that also utilizes the framework to set up the baseline of measurement, but the deviation is obtained indirectly by using an angle-measuring device and a guide rod of fixed-length. These two instruments have the disadvantages of low efficiency and unchangeable chord length. Ono, Numakura, and Odaka developed a device that can be mounted on the inspection train capable of running at 275 km/h. The principle is to measure the distance between the rail and the reference line by using three displacement detectors at intervals of 5 m, but it can only get the result of the versine of a 10 m chord [11].

2) INSTRUMENTS BASED ON THE INERTIAL REFERENCE METHOD

This method is the commonly used and can be further classified into two categories, the direct and indirect inertial reference methods. The direct inertial reference method utilizes an accelerometer to sense the irregularities on the rail surface and calculates its value by double integration of the accelerometer outputs. The indirect inertial reference method utilizes an accelerometer to sense the movements of the measuring carrier and calculate the vertical displacement of the carrier by double integration of the accelerometer outputs; then, by measuring the distance between the rail surface and the carrier, the irregularities of the rail surface can be obtained by adding the distance and the deviation [12], [13]. The instrument, namely, Corrugation Analysis Trolley (CAT), which was developed by RailMeasurement, a British company, can achieve favorable accuracy at a measuring speed of 1 m/s, but we have little knowledge of its inner algorithm and it is too expensive to use in China [13], [14]. Yu developed an instrument that detects short-wave irregularities using the direct inertial reference method, which can measure irregularities with a wavelength smaller than 1.3 m at an accuracy of 0.07 mm [8]. Japanese researchers have determined rail surface roughness by analyzing the outputs of accelerometers installed on the axle box of an inspection car, and has been successfully applied to the actual track inspection work [15]. Liu, Du, and Yang developed a rail corrugation detection system, namely, RCIU-1 using the indirect inertial reference method. This instrument can provide the amplitude of the rail surface irregularities and the standard deviation (SD) of the rail surface roughness, but its accuracy is unknown [16]. Gilbert and Wirksworth utilize an accelerometer and a displacement transducer to monitor the alignment of railway tracks. Double integration of the acceleration outputs in conjunction with the signals from the displacement transducer facilitates the determination of the effective lateral [17]. Weston. P F. *et al.*, used sensor sets, including accelerometers, rate gyros, and displacement transducers, to measure vertical and lateral alignment of the track. The axle box accelerometers are used to measure short wavelengths irregularities while the pitch rate gyro is used to obtain the long wavelength irregularities, this research finding provides an effective way to reconstruct the vertical and lateral track geometry [18], [19]. Tsunashima H. *et al.*, also utilizes a set of sensors to measure track irregularities, wherein vertical

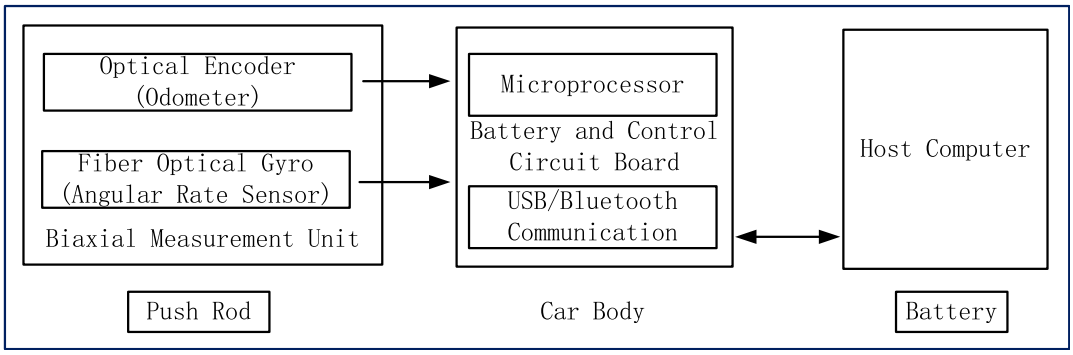

FIGURE 3. Structure and internal workflow of the instrument.

and lateral irregularities are estimated from the acceleration of the car body, the roll angle is obtained by using a rate gyroscope that is used to distinguish line irregularities from level irregularities, and the cabin noise is used to detect the rail corrugation. This device is already installed in six N700 train sets working on Tokaido shinkansen in Japan [20].

This type of instrument can usually move at a relatively high speed but requires complicated algorithms to process the outputs, and its accuracy is heavily affected by the detection speed.

3) INSTRUMENTS BASED ON LASER OR VISIUAL MEASUREMENT METHODS

Mandriota *et al.* [21] proposed a technique, based on Gabor filters and texture analysis of rail surface, to detect and classify rail corrugation. KLD Labs, USA, developed a vehicle-mounted rail-wear measurement system namely ORIAN (Optical Rail Inspection and Analysis), which utilizes two ultra-high-pixel-density digital cameras and two-line lasers to obtain the profiles of transverse sections, instead of the profile in the longitudinal direction [22]. Liu [23] utilized the visual inspection technique and an image processing algorithm to measure the rail wear, and also obtain the profiles of transverse sections only. Li, Tan, and Zhang developed a system for the detection of rail corrugation, which includes an on-board image acquisition subsystem and a corrugation identification subsystem. The rail corrugation is identified based on local frequency features [24]. The shortcoming of the system is that it cannot obtain the specific quantitative indicators of rail irregularities.

C. WORK PRESENTED IN THIS STUDY

In this study, we utilized a fiber optical gyroscope (FOG) and an odometer as the core sensors and developed an instrument to efficiently detect the short-wave irregularities and provide irregularities under any specified chord length. Additionally, it is portable and can be easily installed on other track inspection equipment. While the instrument moves along the rail surface, the existence of track irregularities can lead to the change of the pitch angle of the measuring unit, which can be sensed by FOG. The mileage of the instrument is concurrently measured by the odometer. Then, the change rate of the pitch angle and the forward velocity of the instrument are used to assess the condition of the rail surface, including track irregularities and defects, simultaneously. In the post-processing process, the forward and reverse dead-reckoning (DR) technique is utilized to calculate more accurate values of deviations under different chord lengths; however, these values are not theory based because of the effects of the transfer function. We analyzed the influence of the transfer function and developed a novel method to eliminate its influence, which will be discussed in a later section.

II. IMPLEMENTATION OF THE DETECTION SYSTEM

In this section, the implementation of the detection system is examined with regards to two aspects, the hardware and software.

A. WORK PRINCIPLE OF THE DETECTION SYSTEM

The components of this rapid detection system can be divided into two categories: the hardware and the data-processing part. The whole structure and internal workflow of the detection system is briefly introduced in Figure 3.

The hardware part mainly consists of the car body, the biaxial measurement unit, power-transformers, the control circuit board, and the host computer. The data reception and time synchronization are realized by the control circuit board. The data storage, pre-processing, real-time display, warning, and post-processing are performed by the host computer. The communication between the control circuit and the host computer is realized by the serial port RS422, and the observation data of the odometer and FOG are transmitted to the control circuit board through pulse signals and the serial port RS422, respectively.

B. BIAXIAL MEASUREMENT UNIT

The biaxial measurement unit is the core of the whole system and the embodiment of the fundamental principles used in this study. The structure and photographs of the biaxial measurement unit are shown in Figure 4 and 5, respectively.

The size of biaxial measurement unit is 20 cm $\times$ 15 cm $\times$ 10 cm, it is portable and can be easily installed on other track

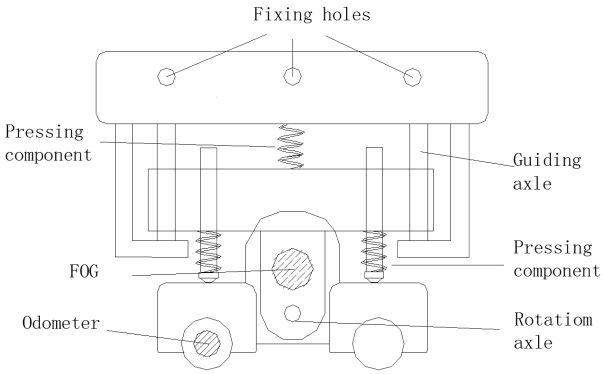

FIGURE 4. Structure of the biaxial measurement unit.

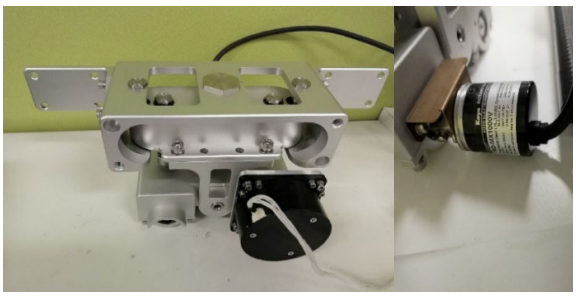

FIGURE 5. Photographs of the biaxial measurement unit. (a) Gyroscope and (b) odometer.

inspection equipment. In Figure 6, show the FOG (black) and the odometer of the biaxial measurement unit represented by (a) and (b), respectively. Although the FOG is not installed in the designated position of the unit because of its size, and that does not affect the results of test.

The two wheels of the biaxial measurement unit maintain contact with the rail surface under the joint action of the guiding axle and the pressing component; to a particular extent, this is similar to the interaction condition between the train wheel and the track. While it is operating, irregularities on the rail surface lead to changes in the unit's pitch angle, which can be measured by FOG and transmitted to the host computer.

The specifications for the FOG are shown in Table 1.

C. SOFTWARE OF THE DETECTION SYSTEM

The software of the detection system can be divided into two parts: the real-time processing part and the post-processing part. Their interfaces are described in the following sections.

1) REAL-TIME PROCESSING

The main interface of the real-time processing software is shown in Figure 6.

The main interface includes the selection of the serial port and data display in text form. Furthermore, the deformation index (DI), and deviation value can be displayed simultaneously on the main interface in graphic form while the

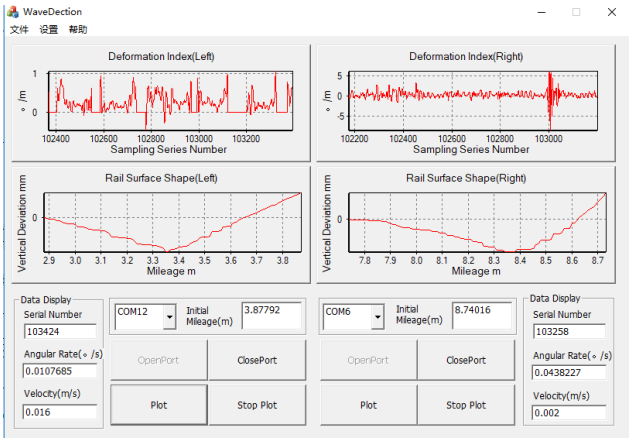

FIGURE 6. Example of main interface of real-time processing software.

TABLE 1. Specifications of FOG.

Bias Stability (Normal Temperature)	⩽ 0.5 °/h
Coefficient of Random Walk Error	⩽ 0.03 °/√h
Nonlinearity of Scale Factor	⩽ 200 ppm
Measuring Range	⩾ ± 300 °/s
Resolution	⩽ 0.01 °/s
Noise Bandwidth	⩽ 0.05 °/s
Working Temperature Range	-40 ℃~+60 ℃

instrument is operating. This is intended to monitor the working state of the device and give real-time information about the geometric state of the rail surface, and an acoustic or photoelectric alarm is generated, if the deviation exceeds the threshold.

2) POST-PROCESSING

The four major interfaces of the post-processing software are shown in Figure 7.

Interface (a) realizes functions including data reading, gross error detection for the outputs of the odometer, preprocessing of the angular rate, and calculation of the deviation with the DR algorithm. The list box on the left shows the raw data while the list box on the right shows the detected gross errors of mileage or the irregularities of rail surface, textboxes on the bottom shows the basic information of observations and calculation results. Interface (b) utilizes the DI to evaluate the rail surface roughness (picture box on the upper part) and can also determine the wavelength of the track irregularities by performing spectrum analysis of the DI (picture box on the lower part). Interface (c) convert the original irregularities (picture box on the upper part) into the true irregularities (picture box on the lower part) by eliminating the influence of the

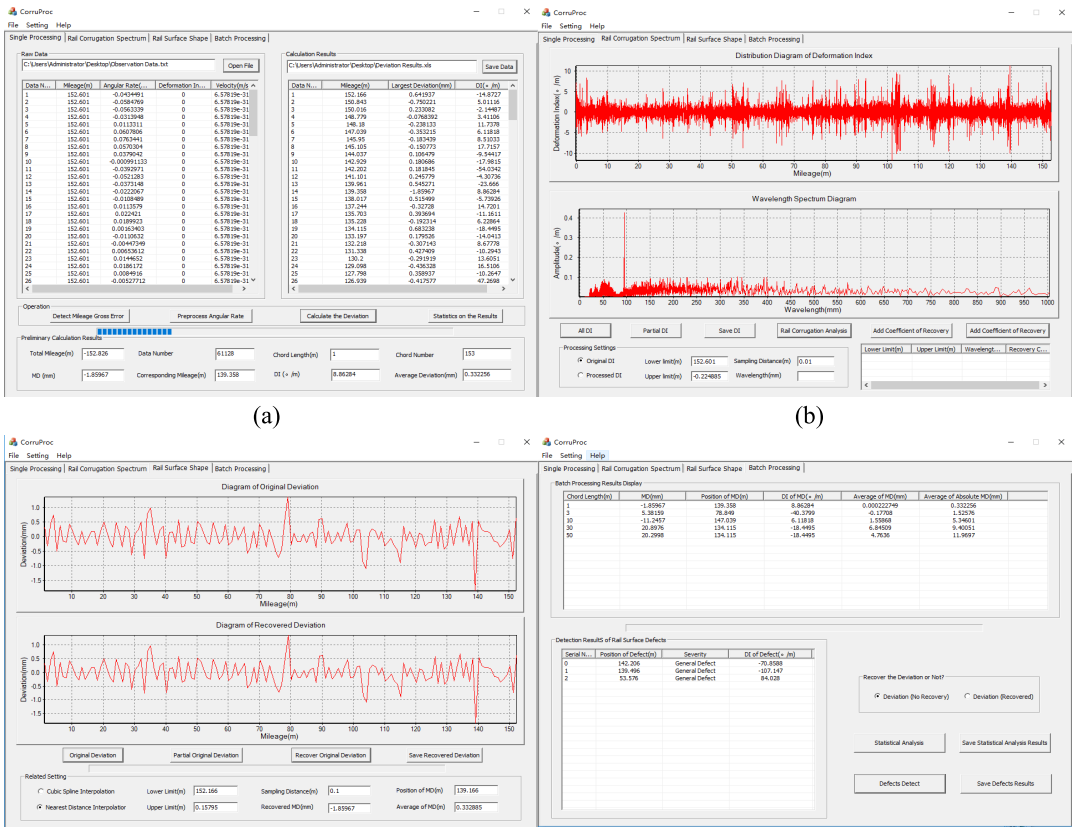

FIGURE 7. Interfaces of post-processing software.

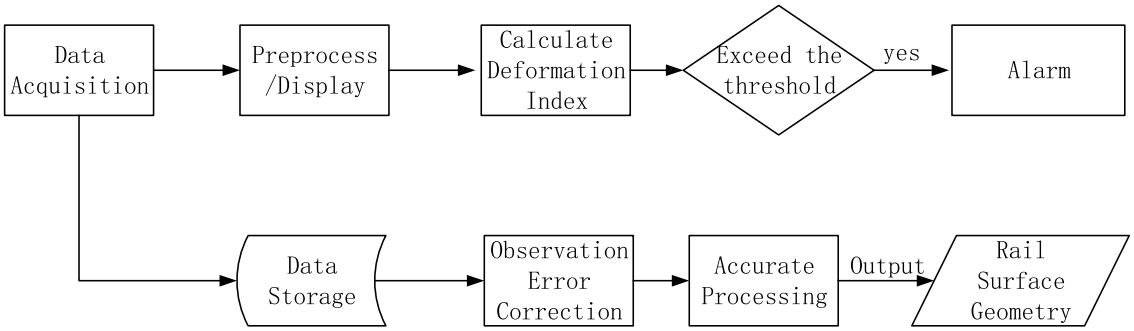

FIGURE 8. Workflow of the detection system.

transfer function when the wavelength has been determined by interface (b), textboxes on the bottom shows the basic information of the calculation results. Interface (d) outputs the statistical results of rail surface irregularities under a specified series of wavelengths (picture box on the upper part) and can also provide the rail defects detected by using the DI (the bottom left corner of the interface).

III. DATA PROCESSING TECHNIQUES

A. WORKFLOW OF THE DETECTION SYSTEM

The workflow of the detection system is shown in Figure 8.

The host computer initializes the system, and subsequently the instrument moves along the rail in the longitudinal direction and samples the FOG and odometer data at regular time intervals. The measured data are transmitted to the host computer followed by storing for post-processing, and also displayed on the screen of the host computer to monitor the state of the rail surface. The ratio of the angular rate to the velocity is used as an indicator to evaluate the severity of rail surface irregularities, and an acoustic or photoelectric alarm is produced if the indicator exceeds the threshold. During post-processing, the data are first pre-processed, and then

the geometric information of the rail surface is calculated by utilizing more complicated and accurate algorithms.

B. MATHEMATICAL MODEL OF DETECTION

1) PRINCIPLES OF DEFECT DETECTION

Irregularities on the rail surface lead to the change of the pitch angle of the biaxial measurement unit, and the angular rate is influenced by the velocity of the instrument, along with the amplitude and wavelength of track irregularities. This can be outlined as follows: the longer the wavelength, the smaller the angular change rate is (on the condition that the velocity of the device and the amplitude of rail corrugation are constant), or the larger the amplitude, the larger the angular rate is (on the condition that the velocity of the device and the wavelength of track irregularities are constant). Thus, the ratio of the angular change rate to the velocity is used as the DI, which is employed to evaluate the state of the rail surface.

$$\mathrm{DI} = \omega / v \tag{1}$$

In formula (1), ω denotes the angular rate of the pitch angle, which is the output of FOG and is expressed in degrees per second; v represents the velocity of the instrument(the output of the odometer), and measured m/s SI unit; and the DI is expressed in degrees per meter. It is obvious that the influence of the velocity has been eliminated.

The DI also represents the magnitude of angular change per unit distance, which can reflect the severity of rail surface irregularities. Defects existing on the rail surface lead to a sudden increase in the DI, and the larger the value of the DI, the greater the impact on the car body. Thus, the DI can be used to evaluate the roughness of the rail surface and detect existing defects.

To avoid an unrealistic result of formula (1) when the velocity is 0 or small, different situations must be taken into consideration:

- The instrument is considered to be stationary when the absolute value of the velocity is smaller than a threshold $v_{\min}(v_{\min} > 0)$; in this case, there is no real-time warning. The determination of $v_{\min}$ requires a comprehensive analysis of various factors, including the precision of the odometer, the required accuracy of the detection, and the actual working conditions.
- The instrument is considered to be in motion when the absolute value of the velocity exceeds the threshold $v_{\min}(v_{\min} > 0)$. Then, the DI is calculated to evaluate the geometric state of the rail surface.

2) PRINCIPLES OF THE CALCULATION OF IRREGULARITIES

The chord length must be specified to calculate the irregularities by using the DR algorithm. Because the outputs of FOG and the odometer are synchronized, the observations can be divided into different segments with selected chord length according to the mileage. The principle of the DR algorithm for the calculation of irregularities is illustrated in Figure 9.

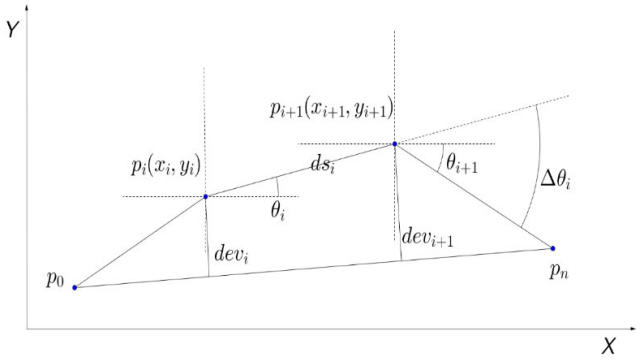

FIGURE 9. Principle of DR algorithm for the calculation of irregularities.

In Figure 9, p_0p_n is the measurement baseline and dev_i and dev_{i+1} are the irregularities of points $p_i\,(x_i, y_i)$ and $p_{i+1}(x_{i+1}, y_{i+1})$, respectively.

The formula of the forward DR algorithm is:

$$\begin{cases} \mathrm{x}_{i+1} = \mathrm{x}_i + ds_i \cdot \cos\theta_i \\ \mathrm{y}_{i+1} = \mathrm{y}_i + ds_i \cdot \sin\theta_i, \end{cases} \quad (i = 1, 2 \ldots n)$$
$$\theta_{i+1} = \theta_i + \Delta\theta_i \tag{2}$$

The formula of the reverse DR algorithm is:

$$\begin{cases} \mathrm{x}_i = \mathrm{x}_{i+1} - ds_i \cdot \cos\theta_i \\ \mathrm{y}_i = \mathrm{y}_{i+1} - ds_i \cdot \sin\theta_i, \end{cases} \quad (i = n, n-1, \ldots 1)$$
$$\theta_i = \theta_{i+1} - \Delta\theta_i \tag{3}$$

In formula (2) and (3), x_i and y_i denote the mileage in the longitudinal direction and the irregularity in vertical direction, respectively, at sampling point i. x_{i+1} and y_{i+1} have the same meaning, but at sampling point $i + 1$. ds_i and θ_i are the mileage increment and pitch angle between sampling points i and $i + 1$, correspondingly. The pitch angles at the start point, θ_1, and the end point, θ_n, in every chord are 0.

Combining the first half of the forward calculation results and the second half of the backward calculation results can reduce the calculation distance by half when compared with the unidirectional DR algorithm. In a way, it can also reduce the accumulation of errors, especially the high frequency noise for the pitch angle is obtained by integrating the angular rate.

After the above calculation process, the mileage x_i and deviation y_i at every sampling point within a chord can be obtained, and the geometry of the rail surface can be reconstructed. Then, the first point and last point are connected with a line segment and the distance from each sampling point to this line segment is calculated—this distance is the irregularity [25].

C. ACCURACY ANALYSIS AND ERROR CORRECTION

1) ANALYSIS OF THE INFLUENCE OF TRANSFER FUNCTION

- Principle of transfer function

The measured value of the irregularity is not equal to the theoretical value. This is not due to the existence of errors,

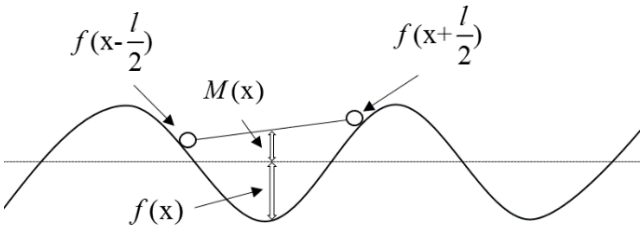

FIGURE 10. Principles of the transfer function.

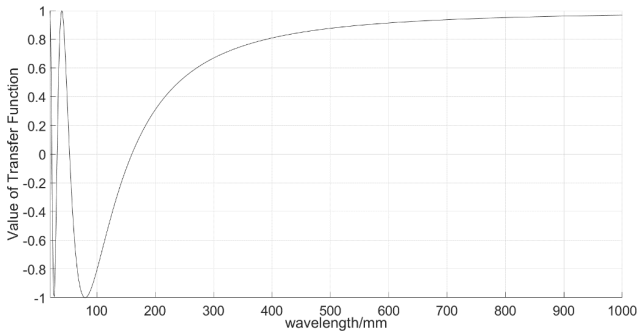

FIGURE 11. Relationship between the transfer function and the wavelength of track irregularities.

but caused by the relationship between the structure of the device and the character of track irregularities [8], [26]. The ratio of the measured value of the irregularity to its theoretical value varies from different wavelengths and amplitudes. Figure 10 shows the principles of the transfer function.

The geometry of rail surface with irregularities can be represented by a sinusoidal function as follows:

$$f(x) = A\sin(\frac{2\pi}{\lambda}x) \tag{4}$$

In the above formula, $f(x)$ is the true value of the deviation, and A, λ are the amplitude and wavelength, respectively.

The measured value of the deviation, $M(x)$, is expressed as follows:

$$M(x) = \frac{A}{2}\left[\sin\frac{2\pi}{\lambda}(x-\frac{l}{2}) + \sin\frac{2\pi}{\lambda}(x+\frac{l}{2})\right] \tag{5}$$

In formula (5), l is the distance between the front wheel and the rear wheel of the biaxial measurement unit, which equals 80 mm. Hence, the transfer function, $H(x)$ can be obtained by the following formula:

$$H(x) = M(x)/f(x) = \cos(\frac{\pi l}{\lambda}) \tag{6}$$

From the above formula, we know that the value of the transfer function is only related to the wavelength of track irregularities when l is fixed.

The relationship between the value of the transfer function and the wavelength of irregularity is shown in Figure 11.

From Figure 11, we know that the ratio of the measured irregularity to the theoretical irregularity is not 1, which means that they are not equal. However, as the wavelength increases, the ratio approaches 1. When the wavelength is larger than 400 mm, the ratio is larger than 0.8, which means that the measured irregularity is very close to the theoretical value. However, the influence of the transfer function needs to be eliminated when track irregularities with a short wavelength exists. The method is described in subsequent section.

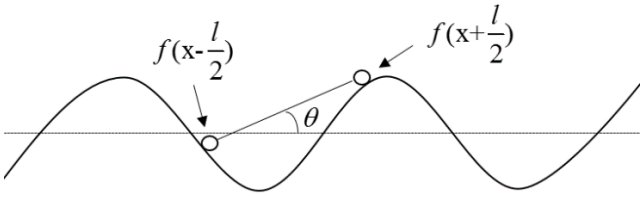

FIGURE 12. Principle of angular rate calculation.

- Influence of the transfer function on the angular rate

The principle used to calculate the angular rate is shown in Figure 12.

The vertical distance of the front wheel is:

$$f(x+\frac{l}{2}) = A\sin\frac{2\pi}{\lambda}(x+\frac{l}{2})$$

The vertical distance of the rear wheel is:

$$f(x-\frac{l}{2}) = A\sin\frac{2\pi}{\lambda}(x-\frac{l}{2})$$

The sine of the pitch angle of the biaxial measurement unit is:

$$\sin\theta = A\left[\sin\frac{2\pi}{\lambda}(x+\frac{l}{2}) - \sin\frac{2\pi}{\lambda}(x-\frac{l}{2})\right]/l$$

Because the track irregularity is very small, the pitch angle is equal to the sine value.

$$\theta \approx \sin\theta = \frac{2A}{l}\cos(2\pi\frac{x}{\lambda})\sin\pi\frac{l}{\lambda} \tag{7}$$

Then, by replacing x with $\boldsymbol{v}\cdot\boldsymbol{t}$ (where $\boldsymbol{v}$ and $\boldsymbol{t}$ are the velocity and time, respectively), we obtain:

$$\theta = \frac{2A}{l}\cos(2\pi\frac{v\cdot t}{\lambda})\sin\pi\frac{l}{\lambda} \tag{8}$$

The derivative of the angle is the angular rate:

$$\dot{\theta} = -\frac{4\pi A}{l\lambda}v\sin\pi\frac{l}{\lambda}\sin(2\pi\frac{v\cdot t}{\lambda}) \tag{9}$$

Formula (9) shows that the angular rate keeps changing provided that there are irregularities and the velocity is non-zero.

The largest angular rate is:

$$\dot{\theta}_{\max} = -\frac{4\pi A}{l\lambda}v\sin\pi\frac{l}{\lambda} \tag{10}$$

This rate is related to the velocity, amplitude, and wavelength of track irregularities when l is constant. The influence

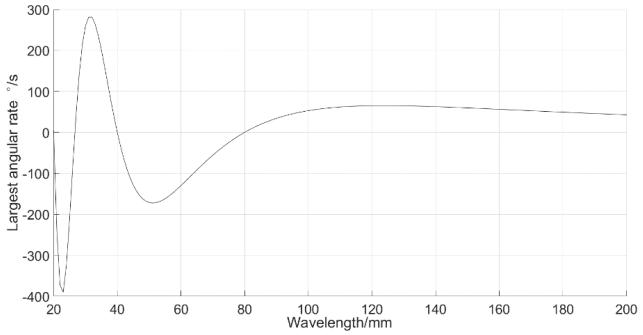

FIGURE 13. Influence of the transfer function on the largest angular rate.

of the transfer function on the largest angular rate is shown in Figure 13.

Figure 13 shows that the angular rate is 0 when the wavelength is 20 mm, 40 mm, and 80 mm. This means that irregularity cannot be detected at these wavelengths.

2) CORRECTION FOR THE INFLUENCE OF THE TRANSFER FUNCTION

In this section, the relationship between the DI and the wavelength of track irregularities is used to correct the influence of the transfer function.

The ratio of angular rate, $\dot{\theta}$, to the velocity, v, is used as the DI, which can be obtained by:

$$\mathrm{DI} = \dot{\theta}/v = -\frac{4\pi A}{l\lambda}\sin\pi\frac{l}{\lambda}\sin(2\pi\frac{v\cdot t}{\lambda}) \tag{11}$$

Because v and t are not constant, the maximum value, $\mathrm{DI}_{\max}$, is obtained when $\sin(2\pi\cdot v\cdot t/\lambda)$ is equal to 1.

$$\mathrm{DI}_{\max} = \frac{4\pi A}{l\lambda}\sin\pi\frac{l}{\lambda} \tag{12}$$

According to the description in references [8], [10], [18], the wavelength and amplitude of track irregularities that usually exist are 300 mm and 1000 mm, respectively, and the corresponding maximum value, $\mathrm{DI}_{\max}$, is:

$$\mathrm{DI}_{\max 300} \approx 22^\circ/m$$

Therefore, the threshold for the detection of defects is 25, which is slightly larger than $N_{\max 300}$.

We replace $\boldsymbol{v}\cdot\boldsymbol{t}$ with $\boldsymbol{x}$ in formula (11) to transform the DI from the time domain to the space domain.

$$\mathrm{DI} = \dot{\theta}/v = -\frac{4\pi A}{l\lambda}\sin\pi\frac{l}{\lambda}\sin(2\pi\frac{x}{\lambda}) \tag{13}$$

Now, the amplitude of the DI changes with mileage when l and λ are fixed; to be specific, the spectrum of the DI is equal to the spectrum of track irregularities because they both have the same wavelength λ. Thus, the wavelength of track irregularities can be obtained through the spectrum analysis of the DI, and then the ratio of the measured irregularity to the theoretical irregularity can be calculated using formula (6) to eliminate the influence of the transfer function.

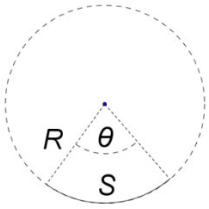

FIGURE 14. The influence of earth's rotation.

3) ANALYSIS OF THE INFLUENCE OF EARTH'S ROTATION

The output of gyroscope is the rotation rate relative to inertial space, thus, the earth's rotation can be projected onto the axis of gyroscope. The angular rate caused by earth's rotation can be considered as a constant value because the direction and elevation of the instrument does not change significantly during detection. The maximum value projected onto the axis of gyroscope is the earth's rotation rate $360^\circ/24h$, assuming that the instrument moves along a flat and straight track, the output of gyroscope is $360^\circ/24h$ (practically it should be 0), which means that the trajectory is a circle after 24 h. The corresponding circumference can be calculated by using the velocity (1 m/s) multiplied by the time (24 h), which gives 86.4 km. The radius R of this circle is 13.75 km.

The versine Δs can be calculated by using:

$$\Delta\mathrm{s} = R(1-\cos(S/2/R)) \tag{14}$$

where S is the chord length and R is the radius. The error caused by earth's rotation or any other constant drift can be calculated by formula (14). Assuming that the chord length is 1 m, the versine that corresponds to earth's rotation is 0.009 mm; if the chord length is 10 m, it is 0.909 mm. The method used to eliminate the influence of earth's rotation is described in later section.

4) ANALYSIS OF GYROSCOPIC DRIFT

The gyroscopic drift is the value of the gyroscope's output when the external input is 0. It can be considered as the difference between the actual value and the real value. When integrating the gyro's outputs, the existence of gyroscopic drift will reduce the accuracy of pitch angle. The gyroscopic drift is defined as follows:

$$\varepsilon = \varepsilon_0 + Asin\,(2\pi ft + \theta_0) + kt + \nabla\,(t) + \Delta(\mathrm{t}), \tag{15}$$

where ε_0 is the constant bias of the gyroscopic drift, A, f, and θ_0 are the amplitude, frequency, and initial phase of the periodical part of the gyroscopic drift, respectively, k is the coefficient of its linear part, $\nabla\,(t)$ is the colored noise, and Δ(t) is the white noise [27]–[29].

We analyzed the error characteristics of FOG by calculating the Allan variance of the output of FOG, which was obtained by sampling for 8 h in a state of rest and at a sampling frequency of 300 Hz.

The raw data in 20 s and the analysis result of all the data by using Allan variance are shown in Figures 15 and Figure 16, correspondingly.

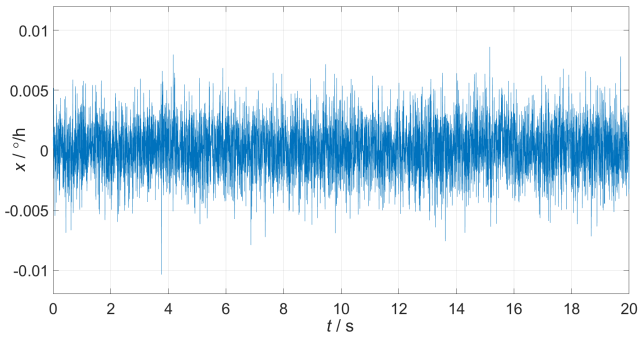

FIGURE 15. Output of FOG in 20 s at a stationary state.

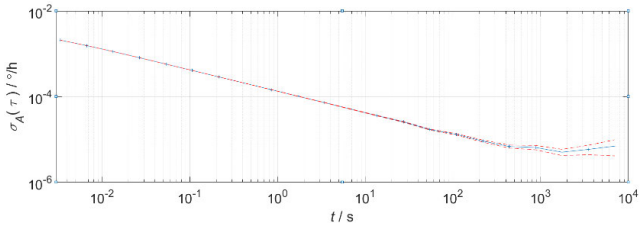

FIGURE 16. Analysis result of the output of FOG by using the Allan variance method.

The existence of different error terms leads to the existence of lines with specific slope in Figure 16, and this feature can be used to analyze the error conditions of the output of FOG [30]–[32].

Most of the curves in Figure 16 are dominated by a straight line with a slope of $-1/2$, which means that white noise is the main part of the gyroscopic drift. However, the problem is that the constant bias cannot be distinguished because of the character of the Allan variance. Therefore, initially we must examine the constant part of the drift before discussing the influence of white noise.

The periodical term can be comprehended by using spectrum analysis method or wavelet transform and the colored noise can be modeled as a first-order Markov process. However, the error model established under static circumstances cannot be utilized for the correction of errors produced on moving conditions, for the time start of the model that cannot be determined. Thus, the next section presents the method for the approximate corrections of other error terms.

5) CORRECTION FOR EARTH'S ROTATION AND THE CONSTANT AND LINEAR PARTS OF THE GYROSCOPIC DRIFT

The influence of high frequency noise of Gyro's outputs is reduced by integrating the angular rate. As described in 3.3.3, the angular rate caused by rotation of the earth can be considered as a constant and has the same effect as the constant bias of the gyroscopic drift. Therefore, we regard the earth's rotation and the constant bias as one constant value. The formula for the calculation of the correction ε_c is:

$$\varepsilon_c = \varepsilon_1 + kt \tag{16}$$

where ε_1 the sum of earth's rotation and the constant is bias of the gyroscope and k is the slope of the linear drift.

If we keep the instrument immobilized for a few minutes before operation, t equals 0, and the correction is:

$$\varepsilon_{c0} = \varepsilon_1$$

If we keep the instrument immobilized for a few minutes after operation, t equals t_e, and the correction is:

$$\varepsilon_{ce} = \varepsilon_1 + kt_e$$

Consequently, the correction ε_c at time t is:

$$\varepsilon_{ct} = \varepsilon_1 + kt_t = [\varepsilon_{c0} \cdot (t_e - t_t) + \varepsilon_{ce} \cdot t_t]/t_e \tag{17}$$

This formula can be used for the correction of earth's rotation and the constant and linear parts of the gyroscopic drift.

6) ANALYSIS OF THE DETECTION ACCURACY

Following the correction discussed in the previous section, the gyroscopic drift can be regarded as a random constant with zero mean white noise; therefore, the SD can be utilized to evaluate the accuracy of the output of the gyroscope. The procedure followed for the accuracy analysis in following steps:

Step 1: The formula for the calculation of the increment of x_i and y_i in one step is:

$$\begin{cases} \Delta_x = \Delta s \cdot \cos\theta \\ \Delta_y = \Delta s \cdot \sin\theta \end{cases} \tag{18}$$

Step 2: The corresponding error equations are as follows:

$$\begin{cases} \delta_{\Delta_x} = \delta_{\Delta s} \cdot \cos\theta - \Delta s \cdot \sin\theta \cdot \delta_\theta \\ \delta_{\Delta_y} = \delta_{\Delta s} \cdot \sin\theta + \Delta s \cdot \cos\theta \cdot \delta_\theta \end{cases} \tag{19}$$

Because the pitch angle θ is very small on the rail surface, the error equation of the increment in the y coordinate (deviation in the vertical direction) can be simplified as follows:

$$\delta_{\Delta_y} \approx \Delta s \cdot \delta_\theta \tag{20}$$

Step 3: θ (the integral of the angular rate) shows the error character of random walk because of the white noise in the angular rate.

Because of the forward and reverse DR utilization, the maximum error will not appear at the middle of a chord, instead, it will appear at 1/4 of a chord length. Thus, the error of θ at 1/4 of a chord is used as the error of the entire stage. Assuming that the chord length is 1 m, the velocity is 1 m/s, and the sampling frequency is 300 Hz, the corresponding data length in the calculation of one chord length is 300 m and the SD of the output shown in Figure 13 is 0.0022° /s. Therefore, the SD of θ at 1/4 of a chord length is:

$$\delta_{\theta_{\text{mid}}} = \sqrt{300/4} \cdot 0.0022 \cdot \pi/180$$

The sampling distance is approximately 0.33 mm and the whole process consists of 300 increments. According to our

FIGURE 17. Experimental conditions.

practical experience, the maximum value of y coordinate often occurs at 1/4 of a chord length; therefore, $\delta_{y_{\max}}$ (the error of the y coordinate at 1/4 of a chord length) is:

$$\begin{aligned}\delta_{y_{\max}} &= \sqrt{300/4} \cdot 0.33 \cdot \delta_{\theta_{\text{mid}}} \\ \delta_{y_{\max}} &= \sqrt{75} \cdot 0.33 \cdot \sqrt{75} \cdot 0.022 \cdot \pi/180 \\ \delta_{y_{\max}} &= 0.009mm\end{aligned}$$

This is the theoretical accuracy that can be obtained by using this rapid detection system when the chord length is 1 m, however for irregularities with wavelength less than 1m, the accuracy can be better.

7) DETECTION OF GROSS ERRORS IN MILEAGE

In case of intense movement or sideslip or outburst errors of the instrument, we utilized the cubic spline curve-fitting method to detect possible gross errors in the mileage. The principle of the cubic spline curve-fitting method can be found in [33]–[35]. The procedure used for gross error detection is as follows:

Step 1: Utilize a certain number of adjacent outputs of the odometer to fit cubic spline curve.

Step 2: Estimate a value in the latest time interval according to the fitted cubic spline curve.

Step 3: Compare the estimated value with the value provided by the odometer, simultaneously. The measured value is considered to be an output with gross error if its difference from the estimated value exceeds a threshold.

The determination of this threshold should be based on the speed of the instrument. Assuming that the highest speed is 2 m/s, then the increment of the mileage during one-time interval is 0.67 cm; the threshold is set as three times this, i.e. 2 cm.

IV. EXPERIMENTAL AND ANALYSIS

A. VERIFICATION OF REPEATABILITY

1) EXPERIMENTAL CONDITIONS

The experiment was performed in the Training Section for Vocational Skills of High-Speed Railways, Wuhan, China. The biaxial measurement unit was provisionally installed on the car body of a different track-inspection instrument, but that did not influence the test results. The experimental conditions are shown in Figure 17.

The rail of the track, shown in Figure 17, was measured five times. The detection device was kept stationary for 5 min before operation and after operation. This was intended to eliminate the influence of the earth's rotation, including the constant and linear parts of the gyroscopic drift. The speed of the detection device was approximately 0.6 m/s in the first three tests and 1.2 m/s in the last two tests; this was intended to increase the complexity of the experimental conditions.

2) VERIFICATION OF DEFECT DETECTION CAPACITY

The DI can reflect the roughness of the rail surface and it is used by the real-time working module, to determine whether there is a defect or not. The irregularities in the first of the five trials was calculated with a chord length of 1 m and displayed in Figure 18 for comparison with the DI obtained from five trials, which is shown in Figure 19. In practice, the DI is sampled in time domain by the frequency of 300 Hz and converted into space domain by resampling in designated distance interval.

The DI obtained from five trials shows a satisfying repeatability. The amplitude of the irregularities increases and do not show a good repeatability where the DI is larger. This is probably because the DI reflects the instantaneous changing character, whereas the track irregularities reflects the periodical and smooth changing character. Although there is a certain relationship between the DI and the track irregularities, they do not correspond well.

From the analysis described in section 2) in part C, the spectrum of the DI is the same as the spectrum of track irregularities. The spectrum analysis is carried on the DI based on five trials, which is shown in Figure 19, and the results are shown in Figure 20.

In general, the horizontal axis represents the frequency in the results of spectrum analysis. But we resampled the DI and converted it into space domain. Now the analysis

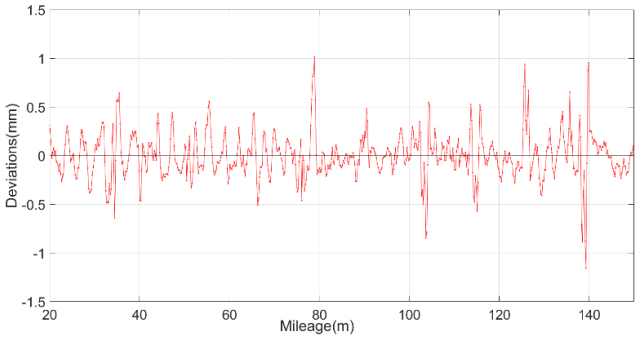

FIGURE 18. Irregularities obtained in the first trials.

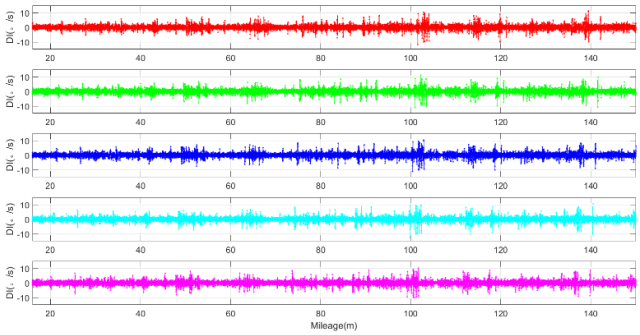

FIGURE 19. DI obtained from five trials.

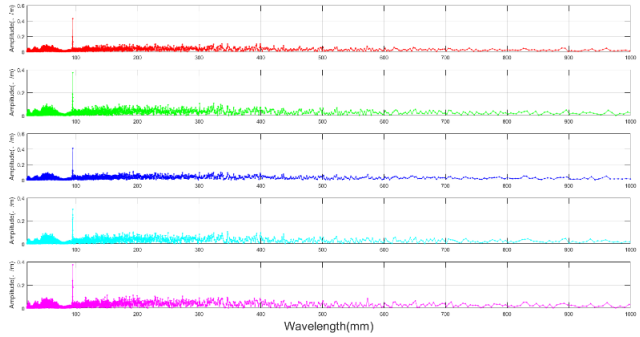

FIGURE 20. Results of spectrum analysis of the DI.

results show the characters of irregularities with different wavelengths. The horizontal axis represents the wavelengths and the vertical axis represents the corresponding intensity. The larger the intensity, the higher the possibility of existence of the irregularity with corresponding wavelength. There is a lower-value section around 80 mm and an obvious peak around 100 mm in the five-measurement spectrum. The reason for the presence of this lower-value section is, the length of the biaxial measurement unit is 80mm, which can filter out irregularities with wavelength is 80 mm. The reason for the presence of the peak is, the encoder was not aligned with the bearing of the wheel (whose circumference is 100 mm), and a slight vibration occurred every time the wheel makes a full turn. This influence has been already eliminated. The dirt attached on the wheels will cause a periodic mutation

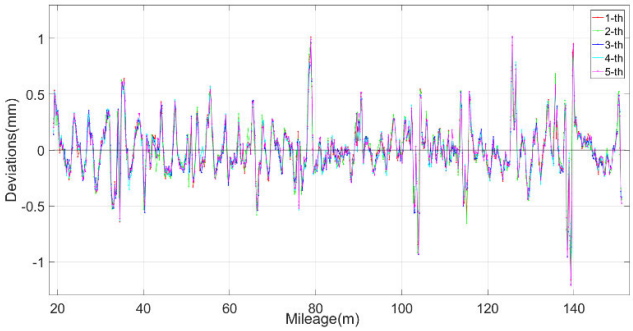

FIGURE 21. Irregularities calculated with a chord length of 1 m.

TABLE 2. Statistics of the irregularities calculated with a chord length of 1 m.

Number of deviations	Number repeatability > 0.1 mm	Percentage repeatability > 0.1 mm
661	22	3.3%
Mean repeatability (mm)	Maximum repeatability (mm)	Minimum repeatability (mm)
0.038	0.425	0.004

in the DI, which is distinguishable and will also appear in Figure 19. The results of spectral analysis of the DI in spatial domain will contain a periodic term with the period is 10 cm, which is equal to the circumference of the wheel.

3) VERIFICATION OF THE REPEATABILITY OF THE ORIGINAL IRREGULARITIES

- Experimental results with a chord length of 1 m

The wavelengths of track irregularities are always smaller than 800 mm [8], [10], [33]. The chord length should be larger than the wavelength, and the sampling interval of the calculated irregularities should be smaller than the wavelength. Therefore, a chord length of 1 m was utilized to calculate the corresponding irregularities and results were obtained in a sampling interval of 20 cm. Irregularities obtained from five trials and calculated with a chord length of 1 m are shown in Figure 21.

The five irregularity curves are very similar to some degree, which means that the repeatability is acceptable. We calculated the repeatability of each point by using its corresponding five irregularities. Other related statistical information is also shown in Table 2.

According to [8], the detection errors of the short-wave irregularities should be lower than 0.1 mm. The number of points with repeatability $>$ 0.1 mm is 22, which accounts for 3.3% of the total. This means that the requirements for detection accuracy can be fulfilled at a probability of 96.7%. The mean repeatability, which is also the repeatability, is 0.038 mm in this test, indicating that this instrument is

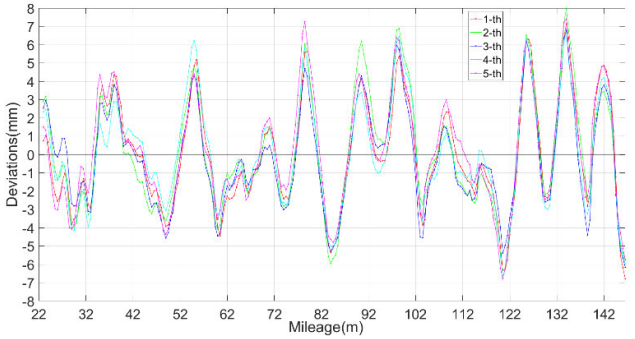

FIGURE 22. Irregularities calculated with a chord length 10 m.

TABLE 3. Statistics of the irregularities calculated with a chord length of 10m.

Number of deviations	Number repeatability > 1 mm	Percentage repeatability > 1 mm
248	18	7.3%
Mean repeatability (mm)	Maximum repeatability (mm)	Minimum repeatability (mm)
0.649	1.152	0.121

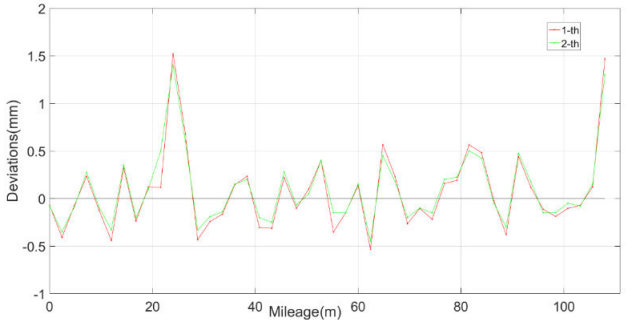

FIGURE 23. Irregularities measured by the two methods.

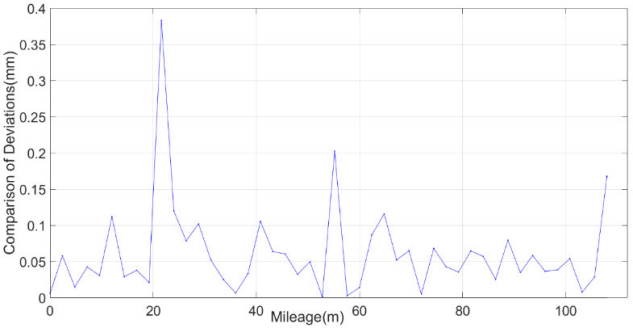

FIGURE 24. The absolute values of differences of the irregularities obtained by using two methods.

sufficiently accurate for the detection of irregularities with a chord length of 1 m.

- Experimental results with a chord length of 10 m

A chord length of 10 m is often used to calculate the irregularity of long wavelengths, thus, the irregularities with a chord length of 10 m and obtained in a sampling interval of 0.5 m from five trials are calculated to verify the performance of this instrument. Results are shown in Figure 22.

The repeatability of the five curves is good except at the position of the peak. The relevant statistical information is shown in Table 3.

To evaluate the detection accuracy with a chord length of 10 m, we used 2 mm as the threshold, as referred in [36]. The number of repeatability smaller than 1 mm is 230, which accounts for 92.7% of the total. The mean repeatability, which can reflect the internal accord accuracy, is 0.649 mm in this test, and it is larger than that acquired when the wavelength is 1m for the irregularities (calculated by using DR algorithm). The larger the wavelength, the more the integral steps, which means that the accumulated errors will be larger, however, the allowance for measurement accuracy will also be larger for longer wavelength. It is still sufficiently accurate for the detection of vertical short-wave irregularities with a chord length of 10 m.

B. VERIFICATION OF EXTERNAL ACCORD ACCURACY

1) EXPERIMANTAL CONDITIONS

This experiment was also performed in the Wuhan Training Section for Vocational Skills of High-Speed Railways, at a different time and track. The irregularities measured by the instrument were compared with independent results obtained manually by using a flat ruler and feeler.

The flat ruler was 1 m long and the thickness of the thinnest piece of the feeler was 0.02 mm. The measuring accuracy should be half of the minimum thickness. Considering the machining accuracy and the influence of the operating conditions, the final accuracy of the irregularities obtained by using the flat ruler and feeler is approximately 0.02 mm.

2) EXPERIMENTAL RESULTS

The comparison of the results is shown in Figure 23.

The red line represents the irregularities measured by the new instrument, and the green line represents the irregularities measured by the combination of the flat ruler and feeler. The two lines are similar, which indicates conformance between the two methods.

The absolute values of the difference between the results of the two methods are shown in Figure 24.

The corresponding DI is shown in Figure 25.

There are severe defects at a distance of approximately 20 m and 60 m in Figure 25, and the corresponding defects are shown in Figure 26 and Figure 27.

The defects shown in Figure 26 and Figure 27 can lead to vibrations of the instrument, decreasing the measuring accuracy in the vicinity of the defects. However, these vibrations would not appear on the rail that is actually used. Therefore, the values affected by severe defects must be eliminated to evaluate the accuracy of the instrument.

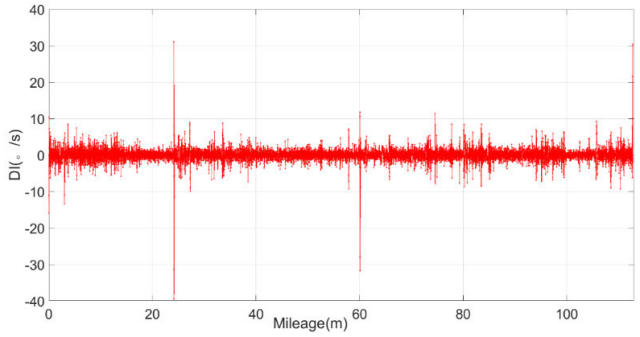

FIGURE 25. The DI.

FIGURE 26. Defects at a distance of approximately 20 m.

FIGURE 27. Defects at a distance of approximately 60 m.

The differences between irregularities obtained by using two methods at i-th point is calculated with formula (21) in the following.

$$\Delta_i = D_I^i - D_m^i$$
$$\Delta_i = (D_I^i - D_R^i) - (D_m^i - D_R^i) \tag{21}$$

D_I^i and D_m^i are the irregularities at i-th point that are obtained by using the developed instrument and the flat ruler or feeler, respectively. D_R^i is the real value of irregularities at i-th point. Assume that δ is the average of absolute value of Δ_i.

$$\delta = \frac{1}{N}\sum_{i=1}^{N} abs(\Delta_i) \tag{22}$$

abs(·) is the function to get absolute value. According to formula (21) and the law of error propagation, formula (23) can be obtained as follows.

$$\delta^2 = (\delta_I^{\mathrm{i}})^2 + (\delta_m^i)^2 \tag{23}$$

δ_I^{i} and δ_m^i are the accuracy of D_I^i and D_m^i respectively. Considering that the measuring accuracy of the flat ruler and feeler δ_{m} is 0.02 mm, the accuracy of the new instrument δ_I can be calculated based on the law of error propagation.

$$\delta_I = \sqrt{0.054 \cdot 0.054\text{-}0.02 \cdot 0.02} = 0.050\mathrm{mm}$$

This accuracy is slightly larger than the repeatability obtained in section 6) in part C because of other types of errors that were not considered in this error calculation. However, it can fulfill the accuracy requirement for measuring the short-wave irregularities, which is described in reference [8] and must be lower than 0.1 mm.

V. CONCLUSION AND DISCUSSION

A. CONCLUSION

In this study, the relevant theory and algorithms were studied in detail to ensure its practicability and accuracy of defects detection and measurement of vertical short-wave irregularities, and the corresponding software was developed for convenience of use.

By using the DI proposed in this study, the real-time working module can detect defects and evaluate the state of the rail surface while the instrument moves along the track. The post-processing module utilizes the forward and reverse DR algorithm and a series of error-correction methods to calculate the irregularities, under any specified chord length and distance interval. The experimental results show that the requirements of detection accuracy can be fulfilled at a probability of 95.8% and the repeatability of the instrument is 0.038 mm when the chord length is 1 m. The repeatability is 0.649 mm and the requirements can be met at a probability of 92.7% when the chord length is 10 m. When compared with the results obtained using a flat ruler and feeler, the accuracy of the new instrument is 0.050 mm. The experimental results confirmed the efficiency and accuracy of the system.

B. DISCUSSION

Although the detection of defects on a rail surface is realized by evaluating the value of the DI, this method cannot distinguish the type of defects. When the biaxial measurement unit passes over a certain type of defects, the DI shows typical characteristics that correspond to this type of defects; thus, the machine-learning algorithm can be applied for the classification of defects.

More types of errors can be considered in the calculation process, to improve the accuracy of the measurement of irregularities.

REFERENCES

[1] H. Yin, H. T. Zhu, Z. Y. Wang, W. J. Wu, and Z. M. Jin, "Rail short-wave irregularity measurement based upon a multi-midpoint chord model," (In Chinese), *J. Vib. Shock.*, vol. 36, no. 14, pp. 178–182 and 193, 2017

[2] *Why Measure Corrugation and Acoustic Roughness*. Accessed: 2018. [Online]. Available: https://cn.bing.com/images/search?q=Rail+corrugation&FORM=HDRSC2

[3] R. B. Faiz and S. Singh, "Condition monitoring of track geometry in UK rail," in *Proc. Int. Conf. Comput., Eng. Inf.*, Fullerton, CA, USA, 2009, pp. 182–190. doi: 10.1109/ICC.2009.9.

[4] H. Ilias and Steffen Müller, "A discrete-continuous track-model for wheelsets rolling over short wavelength sinusoidal rail irregularities," *Vehicle Syst. Dyn.*, vol. 23., pp. 221–233, Apr. 1994.

[5] P.-C. Yu, J. Li, and L.-C. Wang, "Research on the influence of track periodic short-wave irregularity on low-speed maglev train," in *Proc. 35th Chin. Control Conf. (CCC)*, Chengdu, China, 2016, pp. 9305–9310. doi: 10.1109/ChiCC.2016.7554836.

[6] O. Heirich, A. Lehner, P. Robertson, and T. Strang, "Measurement and analysis of train motion and railway track characteristics with inertial sensors," in *Proc. 14th Int. IEEE Conf. Intell. Transp. Syst. (ITSC)*, Washington, DC, USA, Oct. 2011, pp. 1995–2000. [Online]. Available: http://citeseerx.ist.psu.edu/viewdoc/download;jsessionid=3CEC12E842C2C6621DB065EB8D77D4F4?doi=10.1.1.399.3223&rep=rep1&type=pdf
doi: 10.1109/ITSC.2011.6082908.

[7] J. Kawasaki and K. Youcef-Toumi, "Estimation of rail irregularities," *Proc. Amer. Control Conf.*, Anchorage, AK, USA, vol. 5. 2002, pp. 3650–3660. [Online]. Available: http://dspace.mit.edu/bitstream/handle/1721.1/8543/49014676-MIT.pdf;jsessionid=C6C2106DC64F598C3A8E504693F421E2?sequence=2

[8] Z. Yu, "The design of the rail short-wave irregularities measurement system based on the inertia displacement method," (In Chinese), Doctoral dissertation, College Mech. Elect. Eng., Nanchang Univ., Nanchang, China, May 2015.

[9] *Railprof Main Characteristics*. Accessed: 2018. [Online]. Available: http://esveld.com/railprof.html

[10] G. Shen, X. H. Zhang, and M. H. Guo, "Measurement and analysis of rail corrugation on curved track of metro systems," (in Chinese) *Urban Mass Transit.*, vol. 14, no. 4, pp. 53–54, 2011.

[11] S. Ono, A. Numakura, and T. Odaka, "HIGH-speed track inspection technologies," Jr East Tech. Rev., East Jpn. Railway Culture Found., Tokyo, Japan, Tech. Rep., 2003.

[12] R. Gomes, A. Batista, M. Ortigueira, R. Rato, and M. Baldeiras, "Railscan: A tool for the detection and quantification of rail corrugation," in *Proc. Doctoral Conf. Comput., Elect. Ind. Syst.*, Costa de Caparica, Portugal, 2010, pp. 401–408.

[13] H. Tanaka and A. Shimizu, "Practical application of portable trolley for the continuous measurement of rail surface roughness for rail corrugation maintenance," *Quart. Rep. RTRI*, vol. 57, no. 2, pp. 118–124 May 2016.

[14] *Validation of CAT*. Accessed: 2018. [Online]. Available: http://railmeasurement.com/corrugation-analysis-trolley-cat/validation-of-cat/

[15] H. Tanaka, M. Matsumoto, and Y. Harada, "Application of axle-box acceleration to track condition monitoring for rail corrugation management," in *Proc. 7th IET Conf. Railway Condition Monit. (RCM)*, Birmingham, U.K. 2016, pp. 1–7. doi: 10.1049/cp.2016.1191.

[16] L. Lingping, D. U. Heting, and Y. Aihong, "Development of rail corrugation inspection system," (in Chinese) *China Railway Sci.*, vol. 23, no. 6, pp. 65–69, Dec. 2002.

[17] D. Gilbert, "Track monitoring equipment," U.S. Patent 7 081 824 B2, Jul. 25, 2006.

[18] P. F. Weston, P. Li, C. S. Ling, C. J. Goodman, R. M. Goodall, and C. Roberts, "Track and vehicle condition monitoring during normal operation using reduced sensor sets," *HKIE Trans.*, vol. 13, no. 1, pp. 47–54 Jan. 2015. doi: 10.1080/1023697X.2006.10668031.

[19] P. F. Westeon, C. S. Ling, C. Roberts, C. J. Goodman, P. Li, and R. M. Goodall, "Monitoring vertical track irregularity from in-service railway vehicles," *Proc. Inst. Mech. Eng., F, J. Rail Rapid Transit Inst. Mech. Eng.*, vol. 221, no. 1, pp. 75–88 Jan. 2007. doi: 10.1243/0954409JRRT65.

[20] H. Tsunashima, T. Kojima, Y. Marumo, A. Matsumoto, and T. Mizuma, "Condition monitoring of railway track and driver using in-service vehicle," in *Proc. 4th IET Int. Conf. Railway Condition Monit., Derby*, 2008, pp. 1–6. [Online]. Available: https://api.intechopen.com/chapter/pdf-download/34441

[21] C. Mandriota, E. Stella, M. Nitti, N. Ancona, and A. Distante, "Rail corrugation detection by Gabor filtering," in *Proc. Int. Conf. Image Process.*, Thessaloniki, Greece, vol. 2, 2001, pp. 626–628. [Online]. Available: http://static.aminer.org/pdf/PDF/000/319/627/rail_corrugation_detection_by_gabor_filtering.pdf

[22] D. L. Magnus, "Noncontact technology for track speed rail measurements: ORIAN," *Proc. SPIE*, vol. 2458, pp. 45–51, Jun. 1995.

[23] H. Liu, "The method and software implementation of rail wear measurement and real-time surface defects detection," (in Chinese), Ph.D. dissertation, Collage Sci. Eng., Jinan Univ., Guangzhou, Guangdong, China, 2016

[24] Q. Li, Y. Tan, Z. Huayan, S. Ren, P. Dai, and W. Li, "A visual inspection system for rail corrugation based on local frequency features," *2016 IEEE 14th Intl. Conf. Dependable, Autonomic Secure Comput., and 14th Intl. Conf. Pervasive Intell. Comput., and 2nd Intl. Conf. Big Data Intell. Comput. Cyber Sci. Technol. Congr. (DASC/PiCom/DataCom/CyberSciTech)*, Auckland, New Zealand, Aug. 2016, pp. 18–23.

[25] Q. Chen, X. Niu, Q. Zhang, and Y. Cheng, "Railway track irregularity measuring by GNSS/INS integration," *Navigation*, vol. 62, no. 1, pp. 83–93, Mar. 2015.

[26] Shaofeng. Wang, X. Yude, and Z. Yu, "Detection and evaluation of curve corrugation of urban mass transit," (in Chinese), *Urban Mass Transit*, vol. 14, no. 10, pp. 56–60 2011.

[27] W. Tang, S. X. Li, L. Y. Liu, and Y. Yang, "Select of wavelet basis in gyro signal processing," *J. Chin. Inertial Technol.*, vol. 10, no. 5, pp. 28–30, 2002.

[28] W. Fumei, "Researches on the theories and algorithms of the error analysis and compensation for integrated navigation system," (in Chinese), Ph.D. dissertation, School Surveying Mapping, PLA Inf. Eng. Univ., Zhengzhou, China, 2007.

[29] Y. Yang, C. Zhang, J. Lu, and H. Zhang, "Classification of methods in the SINS/CNS integration navigation system," *IEEE Access*, vol. 6, pp. 3149–3158, 2018. [Online]. Available: https://ieeexplore.ieee.org/stamp/stamp.jsp?arnumber=8239787.
doi: 10.1109/ACCESS.2017.2787424.

[30] GROVES and D. Paul, "Principles of GNSS, inertial, and multisensor integrated navigation systems," *Ind. Robot*, vol. 67, no. 3, pp. 101–118, 2013. [Online]. Available: https://ieeexplore.ieee.org/ielx7/62/7062837/07063664.pdf?tp=&arnumber=7063664&isnumber=7062837

[31] E. Buchoud *et al.*, "Enhancement of an optical fiber sensor: Source separation based on brillouin spectrum," *IEEE Access*, vol. 1, pp. 789–802, 2013. [Online]. Available: https://ieeexplore.ieee.org/stamp/stamp.jsp?tp=&arnumber=6656840. doi: .10.1109/ACCESS.2013.2288113

[32] N. El-Sheimy, H. Hou, and X. Niu, "Analysis and modeling of inertial sensors using Allan variance," *IEEE Trans. Instrum. Meas.*, vol. 57, no. 1, pp. 140–149, Jan. 2008. [Online]. Available: http://pdfs.semanticscholar.org/5adc/0b53f0ac30fbe7867df49368ad7d77a79e39.pdf. doi: 10.1109/TIM.2007.908635.

[33] J. A. Adams, "Cubic spline curve fitting with controlled end conditions," *Comput.-Aided Design.*, vol. 6, no. 1, pp. 2–9, Jan. 1974.

[34] Q. Duan, K. Djidjeli, W. G. Price, and E. H. Twizell, "A rational cubic spline based on function values," *Comput. Graph.*, vol. 22, no. 4, pp. 479–486, Aug. 1998.

[35] Z. Habib, M. Sarfraz, and M. Sakai, "Rational cubic spline interpolation with shape control," *Comput. Graph.*, vol. 29, no. 4, pp. 594–605, Aug. 2005.

[36] Department of the Transport Ministry of railways of China, *High Speed Railway Engineering Knowledge Book*, (in Chinese). Beijing, China: China Railway Publishing House, 2011, pp. 117–118.

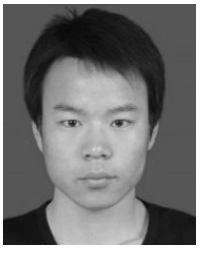

CUIJUN DONG received the B.E. degree in surveying and mapping engineering from the University of Science and Technology at Liaoning, Anshan, Liaoning, China, in 2014, and the M.E. degree in geodesy and surveying engineering from Wuhan University, Wuhan, Hubei, China, in 2017, where he is currently pursuing the Ph.D. degree with the State Key Laboratory of Information Engineering in Surveying, Mapping and Remote Sensing. He has published two second-author papers. His research interests include inertial navigation, integrated navigation, and mobile mapping systems.

QINGZHOU MAO received the Ph.D. degree from Wuhan University, Wuhan, Hubei, China, in 2008.

He has taught at the State Key Laboratory of Information Engineering in Surveying, Mapping and Remote Sensing, Wuhan University, for 12 years, where he is currently a Professor with the School of Remote Sensing and Information Engineering. From 2014 to 2015, he was a Visiting Scholar with PATH, University of California at Berkeley. He has published more than 40 scientific papers. He holds more than 30 patents for invention. His research interests include satellite/inertial navigation, remote sensing and geographic information system (3S) integration technology, intelligent processing technology of laser point cloud and visual data and its application in surveying and mapping of highway, and railway and tunnel engineering.

Dr. Mao has won a second prize of national technological invention and four first prizes of provincial/ministerial level scientific and technological progress.

XIAOCHUN REN received the B.E. degree in railway aerosurveying and the M.E. degree in electronic and information systems from Southwest Jiaotong University, Chengdu, Sichuan, China, in 1984 and 2002, respectively.

Since 1984, he has been with China Railway First Survey and Design Institute Group, Co., Ltd., where he is currently the Deputy Chief Engineer. Since 2016, he has been the Executive Deputy Director of the State Key Laboratory of Rail Transit Engineering Information (FSDI), Xi'an, Shaanxi, China. He has published ten papers and one book. He holds 67 patents for invention. His research interests include precision engineering survey and photogrammetry, and remote sensing technology.

Mr. Ren received the Zhan Tianyou Youth Award and the First Prize of Shaanxi Science and Technology Award.

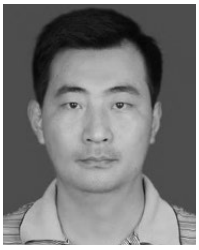

DONGHUA KOU received the B.E. degree in civil engineering and the M.E. degree in traffic and transportation engineering from East China Jiaotong University, Nanchang, Jiangxi, China, in 2004 and 2015, respectively.

He has engaged in professional management of railway line at Wuhan Railway Administration Group Co., Ltd from 2004 to 2018. He is the author of more than 11 articles and has published two books: *Maintenance and Repair of High Speed Railway Ballastless Track* and *Manual Technical of Railway Engineering*. His research interests include inspection, maintenance research, and management of high-speed railway line.

Mr. Kou is currently the Specialty Leading Person of China Railway Corporation. He is also a member of the Standardization (Track) Technical Committee of China Railway Association and the AHG12 Track Quality Inspection Domestic Expert Advisory Group of International Organization for Standardization Railway Application Technical Committee.

JIE QIN received the B.E. degree in railway engineering from Shijiazhuang Tiedao University, Shijiazhuang, Hebei, China, in 2005.

He has engaged in the maintenance and repair of general speed railway at the Wuhan Railway Administration Group Co., Ltd from 2005 to 2010, where he has also engaged in the maintenance and repair of high-speed railway. He has participated in two provincial/ministerial research projects and two bureau-level research projects. He has presided over three bureau-level research projects. He has also participated in the compilation of the book *Maintenance and Repair of High Speed Railway*. He received the Second Prize in Science and Technology of the Railway Academy.

WEI HU received the B.E. degree from Liaoning Technical University, China. He is currently pursuing the master's degree with the State Key Laboratory of Information Engineering in Surveying Mapping and Remote Sensing, Wuhan University. His research interests include satellite/inertial navigation, remote sensing and geographic information system (3S) integration technology, and laser point cloud data processing.